INTERNATIONAL JOURNAL FOR NUMERICAL METHODS IN FLUIDS
Int. J. Numer. Meth. Fluids 2009; **60**:733–751
Published online 9 September 2008 in Wiley InterScience (www.interscience.wiley.com). DOI: 10.1002/fld.1909

Forced-convection heat transfer from tandem square cylinders in cross flow at low Reynolds numbers

A. Sohankar*,† and A. Etminan‡

Department of Mechanical Engineering, Yazd University, Yazd, Iran

SUMMARY

This paper presents the results of a numerical study on the flow characteristics and heat transfer over two equal square cylinders in a tandem arrangement. Spacing between the cylinders is five widths of the cylinder and the Reynolds number ranges from 1 to 200, $Pr=0.71$. Both steady and unsteady incompressible laminar flow in the 2D regime are performed with a finite volume code based on the SIMPLEC algorithm and non-staggered grid. A study of the effects of spatial resolution and blockage on the results is provided. In this study, the instantaneous and mean streamlines, vorticity and isotherm patterns for different Reynolds numbers are presented and discussed. In addition, the global quantities such as pressure and viscous drag coefficients, RMS lift and drag coefficients, recirculation length, Strouhal number and Nusselt number are determined and discussed for various Reynolds numbers. Copyright © 2008 John Wiley & Sons, Ltd.

Received 13 May 2008; Revised 1 July 2008; Accepted 23 July 2008

KEY WORDS: square cylinder; tandem; numerical study; vortex shedding; fluid flow; heat transfer

1. INTRODUCTION

The flow around bluff bodies such as square and circular cylinders is encountered extensively in many structures and industrial applications, e.g. tall buildings, cooling towers, chimneys, pipelines, cables, masts and wires. Flow over a bluff body usually creates a large region of separated flow and a massive unsteady wake region downstream and they have susceptibility to flow-induced vibration. Vortex shedding observed in the wake of these bodies generates unsteady (periodic) lift and drag forces. The fundamental fluid dynamics problems of single circular and square cylinders have been examined extensively in both numerical and experimental studies [1–3]. However, there are not enough results for the flow over the cylinders in tandem, especially with the square cross-section. It seems that there is some similarity between the flow structures of the single and tandem

*Correspondence to: A. Sohankar, Department of Mechanical Engineering, Yazd University, Yazd, Iran.
†E-mail: asohankar@yazduni.ac.ir
‡Current address: Department of Mechanical Engineering, Islamic Azad University, Neyriz Branch, Neyriz, Iran.

bluff bodies. In tandem cases, there are more flow complexities than the single ones because of the existence of two bodies and their reciprocal effect on the flow pattern (spacing effect).

Two-dimensional unsteady flow around the two square cylinders with the different dimensions in a tandem arrangement in a channel has been numerically and experimentally performed by Tatsutani *et al.* [4]. They studied the influence of the distance between the cylinders on the flow structure for Reynolds numbers ranges from 200 to 1600. Their results showed that the flow pattern around the cylinders depends on the distance between the cylinders.

Flow structure and heat transfer from two tandem rectangular cylinders in a channel were numerically simulated by Valencia [5, 6]. It was reported that the drag coefficient and the pressure loss increases due to the existence of the rectangular cylinders in the channel. In addition, the Nusselt number increases on the channel walls by increasing the distance between the cylinders.

Rosales *et al.* [7] numerically simulated the fluid flow and the heat transfer around two square cylinders with different sizes and arrangements in a channel, $Re=500$. In this study, the channel walls and the upstream cylinder are considered insulators whereas the downstream cylinder is hot. It was shown that the drag coefficient and the Nusselt number of downstream cylinder decrease, when the inline or offset tandem pair of cylinders is positioned closer to a channel wall.

Liu and Chen [8] performed an experimental study on the flow over two unconfined square cylinders in a tandem arrangement, $Re=2000$–$16\,000$. They reported that there is hysteresis with two discontinuous jumps, which is associated with two different flow patterns.

The suppression of the fluid forces on the two square cylinders in a tandem arrangement in which a flow approaching the upstream cylinder was controlled by a flat plate was examined, with variation in spacing between the plate and upstream cylinder, $Re=56\,000$ [9].

Two square cylinders were installed in tandem in a vertical water tank and the effects of Reynolds number, spacing ratio and rotation angle of the downstream cylinder on the flow characteristic modes, drag coefficients and the vortex shedding frequency were experimentally studied by Yen *et al.* [10].

Although there are some investigations for the flow over the square cylinders in the tandem arrangements, to the author's knowledge, there are no numerical or experimental heat transfer results in the range of the Reynolds numbers for this study in the published literatures to compare with the present work. The objective of the present work is to study the free-stream flow passing over the two heated tandem cylinders with square cross section for Reynolds number ranges from 1 to 200, $Pr=0.71$.

2. PROBLEM DESCRIPTION, NUMERICAL DETAILS AND THE GOVERNING EQUATIONS

The problem under consideration is depicted in Figure 1. Two equal-sized tandem square cylinders with sides (d) are exposed at zero incidence to a constant free stream with uniform velocity and temperature represented by u_{in}, T_{in}, respectively. Incompressible viscous flow with the constant fluid and heat properties is assumed. All dimensions are scaled with side (d).

The vertical distance between the upper and lower boundaries, H, defines the blockage of the confined flow (blockage parameter, $B=d/H$). It is expected that if the width of the computational domain (H) is chosen adequately large, the lower blockage parameter, the flow in the lower and the upper boundaries goes to the free-stream conditions. In other words, these boundaries should be sufficiently far away from the cylinders to satisfy this boundary condition. In [11], the effect of

DOI: 10.1002/fld

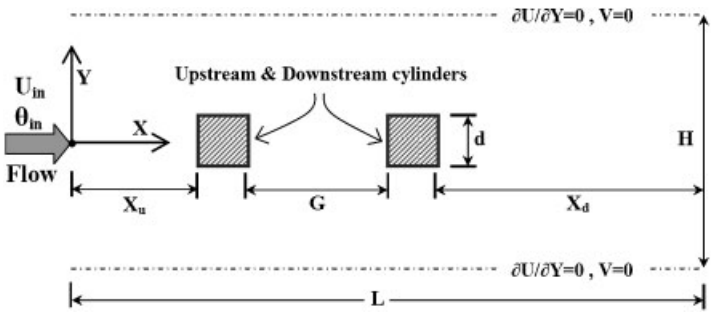

Figure 1. Computational domain for flow around tandem square cylinders.

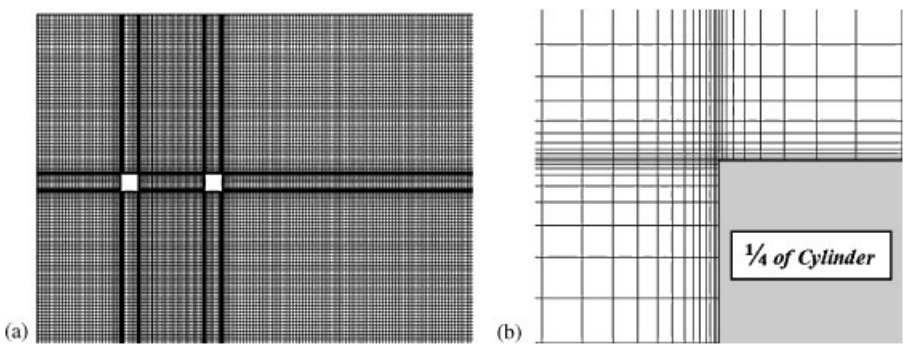

Figure 2. Non-uniform computational grid (220×141): (a) computational domain and (b) close up the cylinder.

blockage was studied for a single square cylinder. They have shown that the free-stream condition is satisfied and that the boundaries have little effect on the characteristics of flow near the cylinder if $B = 5\%$, i.e. $H = 20$. In this work, the blockage study is performed for the present configuration. The distance between the cylinders is selected as a constant value in this work, i.e. $G = 5$, see Figure 1.

In this research, the upstream and downstream distances of the computational domain are selected $X_u = 5$ and $X_d = 15$, respectively, see Figure 1. These values are chosen based on the accomplished studies in the present work and also in [11] to reduce the effect of outlet and inlet boundaries on the flow pattern near the cylinders. It is worth noting that when increasing the upstream extent from $X_u = 5$ to $X_u = 10$, the deviation in the drag coefficient, Strouhal and Nusselt numbers is $-5, -4$ and 6% ($Re = 100$, $B = 5\%$), respectively. A further increase of $X_u = 15$ provides negligible changes in the results. In addition, it is found that an increase from $X_d = 15$ to $X_d = 25$ ($Re = 100$, $B = 5\%$) gives negligible influences in the global quantities (less than 1%).

A typical generated grid is shown in Figure 2. Owing to the existence of the cylinders and their effect on the flow, a non-uniform grid is made around the cylinders using a hyperbolic tangent stretching function. This type of stretching functions and their advantages in non-uniform grid distribution have been discussed by Thompson *et al.* [12]. Beyond this non-uniform region (one d

DOI: 10.1002/fld

from cylinders surfaces), a uniform grid is established with the same size as the latest generated cell in the places with non-uniform grid distribution.

The employed boundary conditions are as follows:

Top and bottom boundaries: $\partial\theta/\partial Y=\partial U/\partial Y=0, V=0$.
No-slip condition and fixed temperature on the cylinders walls: $U=V=0, \theta=1(T=T_{\mathrm{W}})$.
Uniform velocity and temperature at the inlet: $V=\theta=0(T=T_{\mathrm{in}}), U_{\mathrm{in}}=1$.
Outlet boundary condition: $\partial U_i/\partial X=0, \partial\theta/\partial X=0$.

The unsteady governing equations in dimensionless form for incompressible flow and temperature field are given as follows:

$$\text{Continuity: } U_{i,i}=0 \tag{1}$$

$$\text{Momentum: } U_{i,\tau}+(U_iU_j)_{,j}=-P_{,i}+Re^{-1}U_{i,jj} \tag{2}$$

$$\text{Energy: } \theta_{,\tau}+(U_j\theta)_{,j}=(RePr)^{-1}\theta_{,jj} \tag{3}$$

where

$$\tau=\frac{t\,u_{\mathrm{in}}}{d},\quad P=\frac{p}{\rho u_{\mathrm{in}}^2},\quad U_i=\frac{u_i}{u_{\mathrm{in}}},\quad \theta=\frac{T-T_{\mathrm{in}}}{T_{\mathrm{W}}-T_{\mathrm{in}}},\quad i,j=1,2$$

All of the above equations are presented with regard to constant density and viscosity and also negligible viscose dissipation. The Reynolds, Strouhal and Prandtl numbers are defined as $Re=u_{\mathrm{in}}d/\nu$, $St=fd/u_{\mathrm{in}}$, $Pr=\upsilon/\alpha$, respectively, where u_{in}, d and f correspond to the inlet flow velocity, the side of cylinders and the frequency of vortex shedding. In addition, ρ, ν, α are density, kinematic viscosity and thermal diffusion coefficient of the fluid, respectively. T_{in} and T_{w} are inlet temperature and wall temperature, respectively.

An incompressible SIMPLEC finite volume code is used employing collocated grid arrangement. The scheme is implicit in time, and a Crank–Nicolson scheme, which is of second-order has been used. The convective and diffusive terms are discretized using QUICK and central differencing schemes, respectively. The time-marching calculations are commenced with the fluid at rest and a constant time step $\Delta t=0.025$ is used for all simulations. This value is chosen based on the previous works of the first author [11].

3. RESULTS AND DISCUSSION

3.1. Single square cylinder

In order to be confident about the accuracy of the obtained results for the tandem cases, the fluid flow and the heat transfer around a single square cylinder are also studied and their results are compared with the existing results [11, 13–18]. This is because, to the authors' knowledge, there are no numerical or experimental heat transfer results in the published literatures for comparison with the considered Reynolds numbers and the boundary conditions of this study.

Total and pressure drag coefficients, Strouhal number and Nusselt number are presented and compared with the existing results in Figures 3(a)–(d). As can be seen, the agreement between the present results and the others is reasonable and a small deviation between the numerical results

DOI: 10.1002/fld

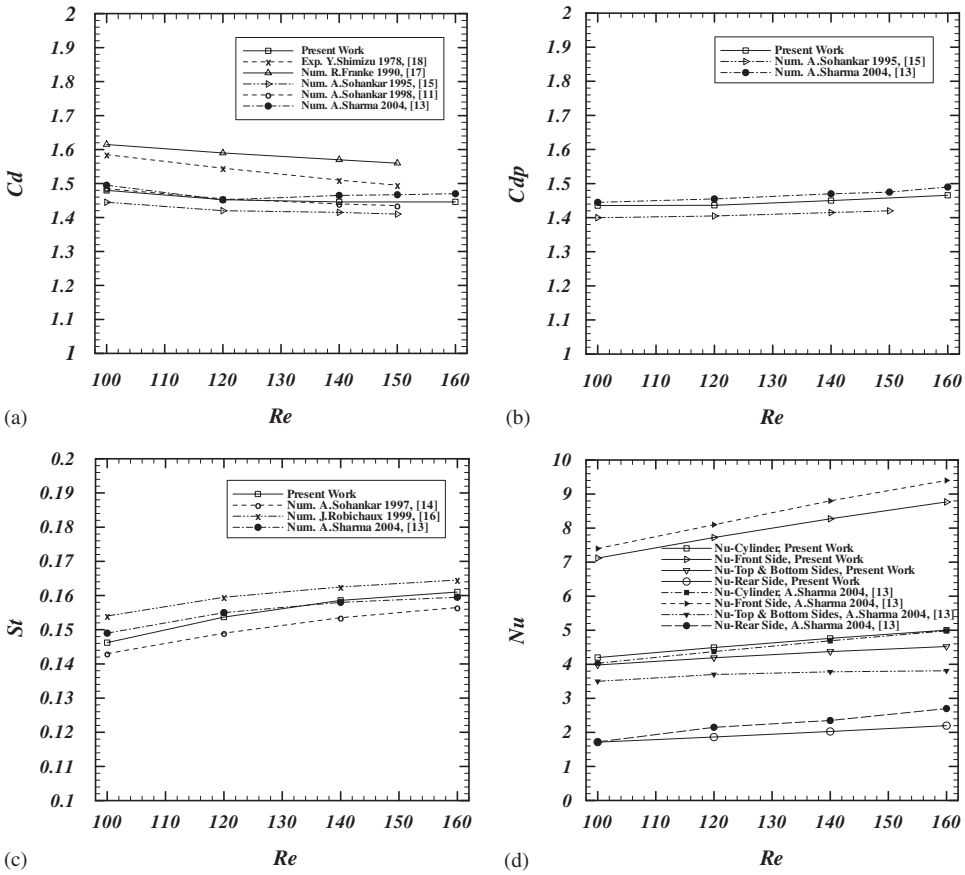

Figure 3. Variation of the: (a) total drag coefficient; (b) pressure drag coefficient; (c) Strouhal number; and (d) Nusselt number, with Reynolds number for single square cylinder.

depends on the different grids used, time step, solution algorithm and so on. For example, the maximum deviation between the obtained Strouhal number and the results of other researches is about 5%.

In Figure 3(d), the total time-averaged Nusselt number and the time-averaged Nusselt numbers for different cylinder sides are compared with the results of Sharma and Eswaran [13]. It is necessary to mention that Nusselt numbers of the upper and the lower sides of the cylinder are the same. As seen, the deviation between the calculated Nusselt numbers and the results of Sharma and Eswaran [13] is small. The maximum deviation between the total (the whole cylinder) Nusselt numbers is about 4.2% and this difference reduces to about 0.4% at higher Reynolds number.

In general, a reasonable agreement is observed between the fluid flow and the heat transfer parameters of this study for the single cylinder with the existing numerical and experimental results. Thus, it is expected that the obtained results for tandem cylinders is also confident.

DOI: 10.1002/fld

3.2. Tandem square cylinders

In this study, three resolutions are employed to test the effect of grid on the results, see Table I. The smallest dimensionless cell established in the vicinity of the cylinders' wall is approximately 0.0053, and the largest in the uniform zones is approximately 0.18. The number of generated cells, in other words, the number of control volumes, has an effect on the results and the run time. As seen from the results in Table I for different grids, the increase in the number of cells in grids II and III has little influence on the results. Based on this refinement study, all further simulations are performed with grid I.

The blockage ratio can have a remarkable effect on the fluid flow and heat transfer patterns around the cylinders and on the different engineering parameters [11]. Blockage ratio is defined as the ratio of the width of the cylinder to the width of the computational domain ($B=d/H$, see Figure 1). Since the upper and lower boundaries are considered frictionless walls ($V=\partial U/\partial Y=0$), choosing a small H causes the velocity field near these boundaries to become uniform, whereas in physical reality the flow around the cylinders needs more space for conformity with these boundary conditions. Using a small H can provide a non-real increase for the effective velocity around the cylinders. This effect causes the Strouhal number to increase and pressure to decrease, especially in the wake zones behind the cylinders, and consequently the drag coefficient increases. This effect is seen clearly in Figure 4, where the time-averaged pressure coefficient distribution around the

Table I. Effect of different resolutions on the flow parameters at $Re=100$ and $G=5$.

		Cl_{rms}		Cd_{rms}		Cd		Cd_P		*St*	
Grid	$(M\times N)$	Up. str. cyl.	Down str. cyl.	Up. str. cyl.	Down str. cyl.	Up. str. cyl.	Down str. cyl.	Up. str. cyl.	Down str. cyl.	Up. str. cyl.	Down str. cyl.
I	220∗141	0.2145	1.5737	0.0072	0.1401	1.534	1.300	1.489	1.155	0.143	0.143
II	253∗163	0.2209	1.5878	0.0076	0.1412	1.537	1.302	1.494	1.158	0.143	0.143
III	298∗196	0.2253	1.5974	0.0078	0.1390	1.539	1.292	1.497	1.150	0.143	0.143

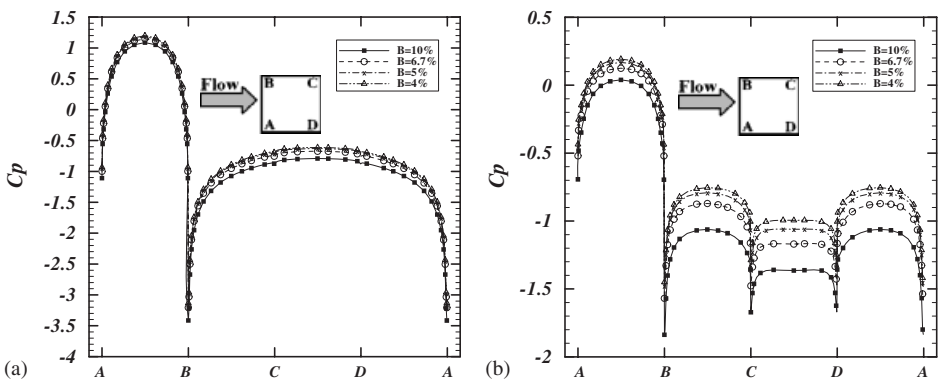

Figure 4. Time-averaged pressure coefficient distribution around the cylinders for different blockage ratios at $Re=100$ and $G=5$: (a) upstream cylinder and (b) downstream cylinder.

DOI: 10.1002/fld

Table II. Effect of different blockage ratios on the flow parameters at $Re=100, G=5$.

	Cl_{rms}		Cd_{rms}		Cd		Cd_P		*St*	
B%	Up str. cyl.	Down str. cyl.	Up str. cyl.	Down str. cyl.	Up str. cyl.	Down str. cyl.	Up str. cyl.	Down str. cyl.	Up str. cyl.	Down str. cyl.
10	0.2108	1.6946	0.0072	0.1514	1.592	1.467	1.547	1.312	0.150	0.150
6.7	0.2069	1.5848	0.0067	0.1542	1.542	1.372	1.497	1.219	0.144	0.144
5	0.2145	1.5737	0.0072	0.1401	1.533	1.300	1.489	1.155	0.143	0.143
4	0.2278	1.5678	0.0076	0.1300	1.534	1.258	1.490	1.118	0.143	0.143

Table III. Effect of different blockage ratios on the Nusselt number at $Re=100, G=5$.

	Nu front side		*Nu* top side		*Nu* rear side		*Nu* bottom side		$Nu_{Cylinder}$	
B%	Up str. cyl.	Down str. cyl.	Up str. cyc.	Down str. cyl.	Up str. cyl.	Down str. cyl.	Up str. cyl.	Down str. cyl.	Up str. cyl.	Down str. cyl.
10	5.13	5.67	3.34	3.29	1.66	1.57	3.34	3.29	3.37	3.46
6.7	5.97	5.73	3.30	3.25	1.67	1.56	3.30	3.25	3.56	3.41
5	5.96	5.53	3.30	3.23	1.67	1.56	3.30	3.23	3.56	3.39
4	5.96	5.52	3.30	3.21	1.67	1.56	3.30	3.21	3.56	3.38

cylinders is shown. It is seen from this figure that the decrease in the blockage ratio from 10 to 4% (or increase of H from 10 to 25) causes an increase in the pressure coefficient. This variation between $B=5\%$ and 4% is negligible.

In Table II, the global flow parameters are shown. It can be seen that a decrease in the blockage ratio from 10 to 5% causes a reduction of 4.7% in the Strouhal number. As mentioned, an increase in the blockage ratio causes an increase in the flow effective velocity around the cylinders. This provides a higher effective Reynolds number and Strouhal number. There are also changes for the other global parameters with the blockage. For example, when the blockage ratio reduces from 10 to 4%, the drag coefficient of the downstream cylinder decreases approximately 13%, see Table II.

The time-averaged Nusselt number for the upstream and downstream cylinders is computed and gathered in Table III for the different blockage ratios. In this table, the total and the cylinder sides Nusselt numbers are provided for upstream and downstream cylinders. By changing the blockage ratio from 10 to 5%, the total Nusselt number decreases to approximately 5.6 and 2% for the upstream and downstream cylinders, respectively. The further decrease of the blockage ratio to 4% produces a negligible change in the Nusselt numbers.

As observed from the presented results (Tables II and III and Figure 4), a decrease in the blockage ratio from 5 to 4% has negligible changes on the fluid flow and heat transfer results. Thus, it is expected that $B=5\%$ is a suitable blockage ratio for further simulations of the present work.

So far, the effects of grid and the blockage on the results have been studied. In what follows, the effect of the parameters such as Reynolds number, which can affect the flow and heat transfer around the tandem square cylinders, will be studied.

In this work, the unsteady flow and heat transfer around two square cylinders in tandem arrangement are studied for $Re=1-200$ at $G=5$. It is observed that the flow is steady for $Re\leqslant 35$ and

DOI: 10.1002/fld

it changes to unsteady for $Re \geqslant 40$ ($B=5\%, G=5$). In the steady cases, the selected Reynolds numbers for the present study are 1, 2, and 5 to 35 in steps of 5 and the chosen Reynolds numbers in the unsteady cases are from 40 to 60 in steps of 5, from 60 to 100 in steps of 10 and from 100 to 200 in steps of 25. For all simulations, the Prandtl number is considered as $Pr=0.71$. In the unsteady flow regime, the time-averaged quantities of the fluid flow and the heat transfer parameters are calculated over approximately 20 shedding cycles in the saturated state where the starting processes are negligible.

3.2.1. Flow and isotherm patterns. Instantaneous streamlines and vorticity contours around tandem cylinders are shown for $Re=100$ in Figure 5. Owing to periodicity of the flow in the fully developed state, where the force signal amplitude reaches approximately to the constant levels, only five instants during the half a shedding period are considered here. It is seen that a clockwise vortex is in development due to the separation at the upper rear corner of the upstream cylinder, see Figure 5(a). As it grows, with increasing strength but being fixed in position, the attachment point on the rear side is pushed downward, see Figures 5(b) and (c). As the attachment point more or less reaches to the lower rear corner at an instance between the corresponding time for Figures 5(c) and (d), a new anti-clockwise vortex is about to be formed at the lower rear corner, see Figure 5(e). As this new vortex grows, the old clockwise vortex is pushed away and is eventually shed into the wake of the upstream cylinder. In general, the same trend is also observed for the other time instants during the next half a shedding period but due to the separation from the lower rear corner.

Figures 6 and 7 show the time-averaged streamlines and vorticity contours around the cylinders for the different Reynolds numbers, respectively. At very low Reynolds numbers, the streamlines stick to both the cylinders' walls completely and flow separation does not occur (see Figure 6 for $Re=1$). As Reynolds number is increased, the flow is not fully attached and separation occurs. In this case, a pair of steady symmetric vortices forms behind the cylinders, see Figure 6(b) for $Re=5$. At higher Reynolds numbers, the formation length of the recirculation region behind the cylinders grows and the vortices become stronger (see Figures 6 and 7). At a critical Reynolds number approximately $Re=40$, flow becomes unsteady and the vortex shedding occurs. For Reynolds number larger than the onset one, the twin vortex arrangement becomes unstable, and a time-periodic oscillation wake and a staggered vortex street are formed from both the cylinders. For $Re \geqslant 40$ ($B=5\%$), the separated vortices are shed alternately from the upper and the lower side of the cylinders, see Figure 5 for $Re=100$. For Reynolds number larger than the critical one, the time-averaged streamlines and vorticity contours are provided, see Figures 6 and 7 for $Re \geqslant 40$. This critical Reynolds number for the single square cylinder is reported in the range of $Re=40$–55 [11, 19]. In general, the critical Reynolds number depends greatly on the distance between the cylinders, inlet flow condition, and the blockage ratio. For example, it is found that the onset Reynolds number for the tandem square cylinders occurs in the range of 35–40, and 40–45 for $B=5\%$ and $B=10\%$, respectively. As mentioned before, the results become independent from the blockage effect for $B \leqslant 5\%$. Thus, it is expected that the accurate critical onset Reynolds number happens at approximately $Re_{cr} \approx 35$–40. In the steady cases, the recirculation length behind the cylinders becomes larger by increasing the Reynolds number and it reaches to the maximum size at the onset Reynolds number, see Figures 6(a)–(e). In all the cases, the recirculation length of the upstream cylinder is larger than the corresponding value for the downstream cylinder. In the unsteady cases, the time-averaged upstream recirculation length decreases with increasing Reynolds number, whereas the corresponding value for the downstream cylinder first decreases and then

DOI: 10.1002/fld

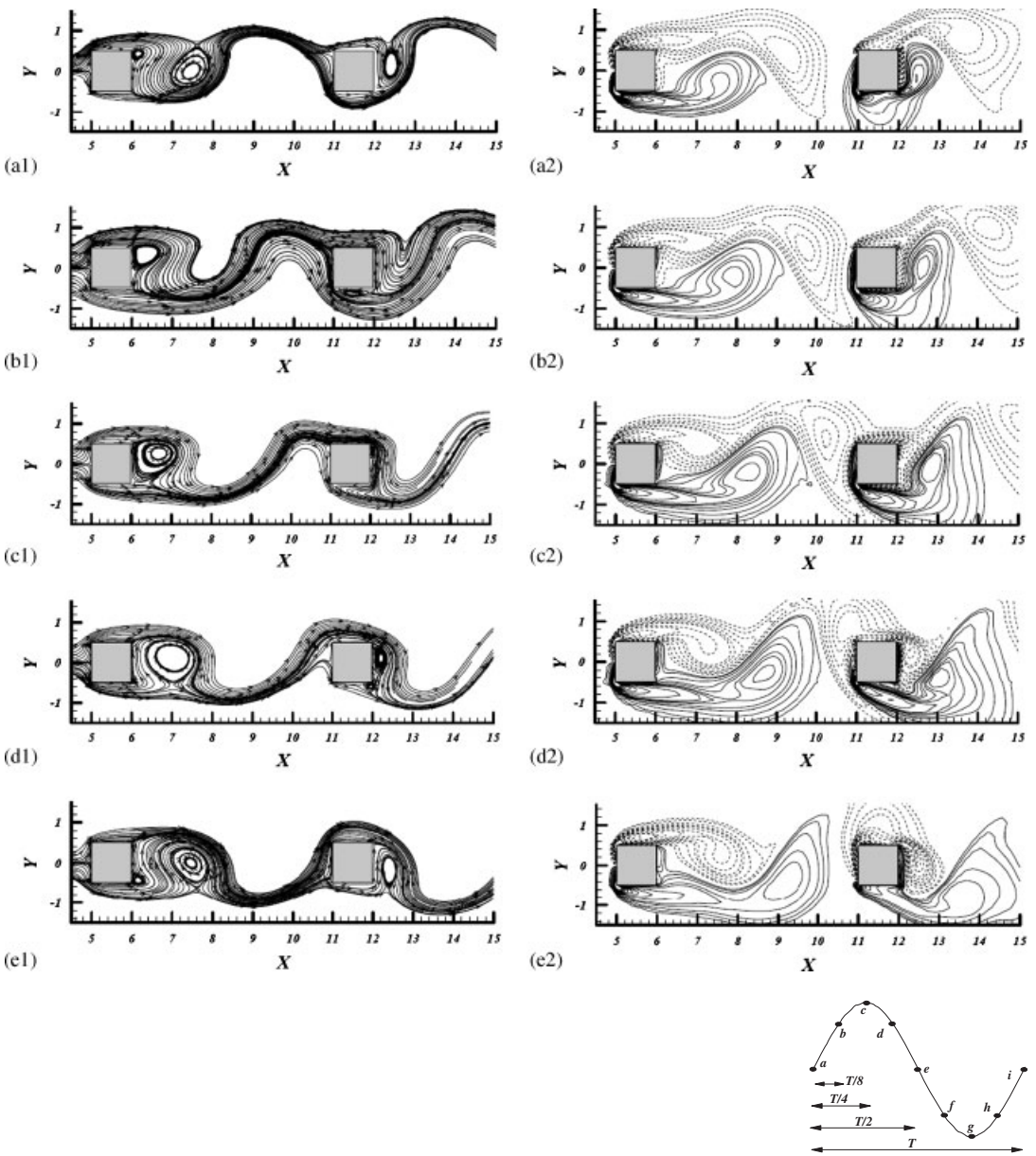

Figure 5. Instantaneous streamlines and vorticity contours for the tandem square cylinders at five instants during half a period of the vortex shedding (see the opposite graph), $Re = 100$ and $G = 5$.

gradually increases. It is reported that the recirculation length for a single square cylinder increases up to approximately the onset of vortex shedding and then decreases [13] and the same trend also occurs for the upstream cylinder in the tandem arrangement.

DOI: 10.1002/fld

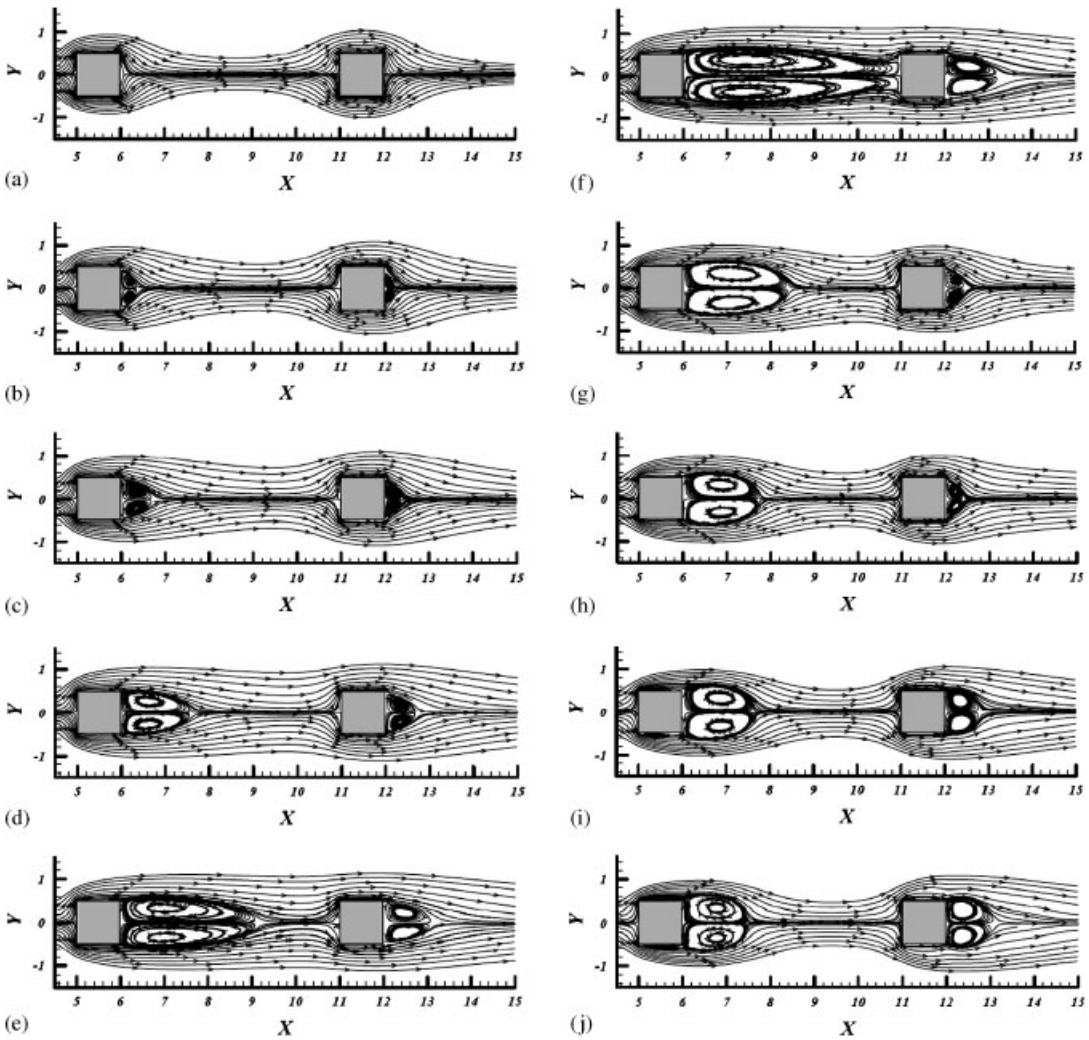

Figure 6. The streamlines around the cylinders for different Reynolds numbers: (a) $Re=1$; (b) $Re=5$; (c) $Re=10$; (d) $Re=20$; (e) $Re=35$; (f) $Re=50$; (g) $Re=70$; (h) $Re=100$; (i) $Re=150$; and (j) $Re=200$. The time-averaged streamlines are shown for the unsteady-periodic flow cases ($Re>35$).

As seen from Figure 7, the level of vorticity is high at the sharp edges of the cylinders. In addition, the level of vorticity is lesser for downstream cylinder than for the upstream one. Vorticity levels greatly increase with the appearance of the vortex shedding at $Re\geqslant 40$.

Figure 8 shows isotherms around the cylinders for different Reynolds numbers in the range of the steady flow regime (8(a)–(e)) and in the unsteady-periodic flow regime (8(f)–(j)). The intensity of the isotherms around the cylinders is similar at low Reynolds numbers, where the streamlines are fully attached and no separation occurs, see Figures 6 and 8 for $Re=1$. This intensity becomes more non-uniform around the cylinders, when the Reynolds numbers increase from $Re=1$ due to flow separation. As seen from Figure 8, there is the crowding of isotherms on the front face of

DOI: 10.1002/fld

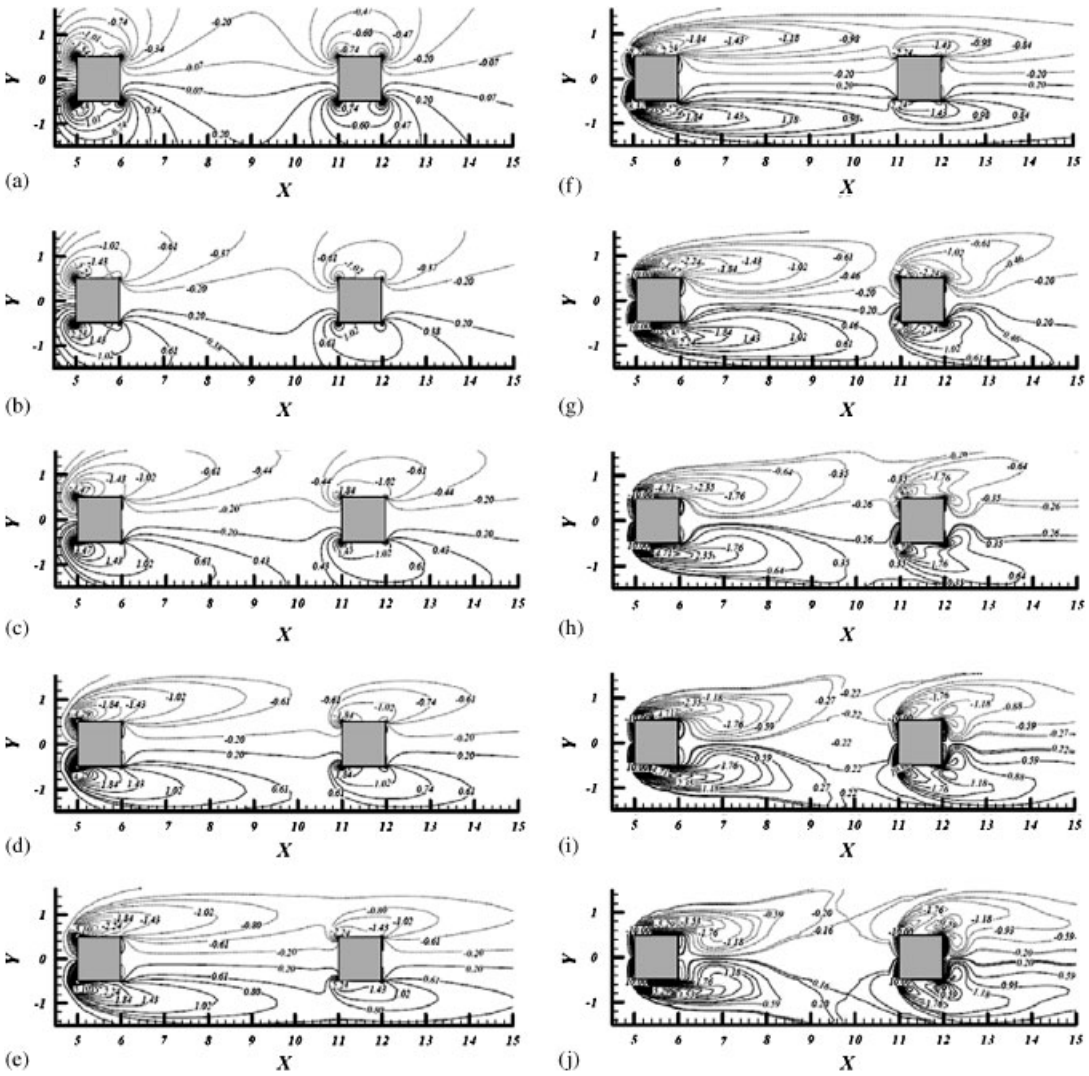

Figure 7. The vorticity contours ($\omega_Z = \pm 10$) around the cylinders for different Reynolds numbers: (a) $Re = 1$; (b) $Re = 5$; (c) $Re = 10$; (d) $Re = 20$; (e) $Re = 35$; (f) $Re = 50$; (g) $Re = 70$; (h) $Re = 100$; (i) $Re = 150$; and (j) $Re = 200$. The time-averaged contours are shown for the unsteady-periodic flow cases ($Re > 35$).

the cylinders especially for the upstream one at higher Reynolds numbers. This indicates a higher heat rate or heat transfer coefficient. Such a crowding of isotherms is not observed over the other faces where the flow separation and wake occur at the higher Reynolds numbers.

3.3. Global quantities

As mentioned earlier, the steady flow becomes an unsteady-periodic flow for $Re \geqslant 40$, and the alternative forces exert on the cylinders. This is clearly seen in Figure 9, where the time history

DOI: 10.1002/fld

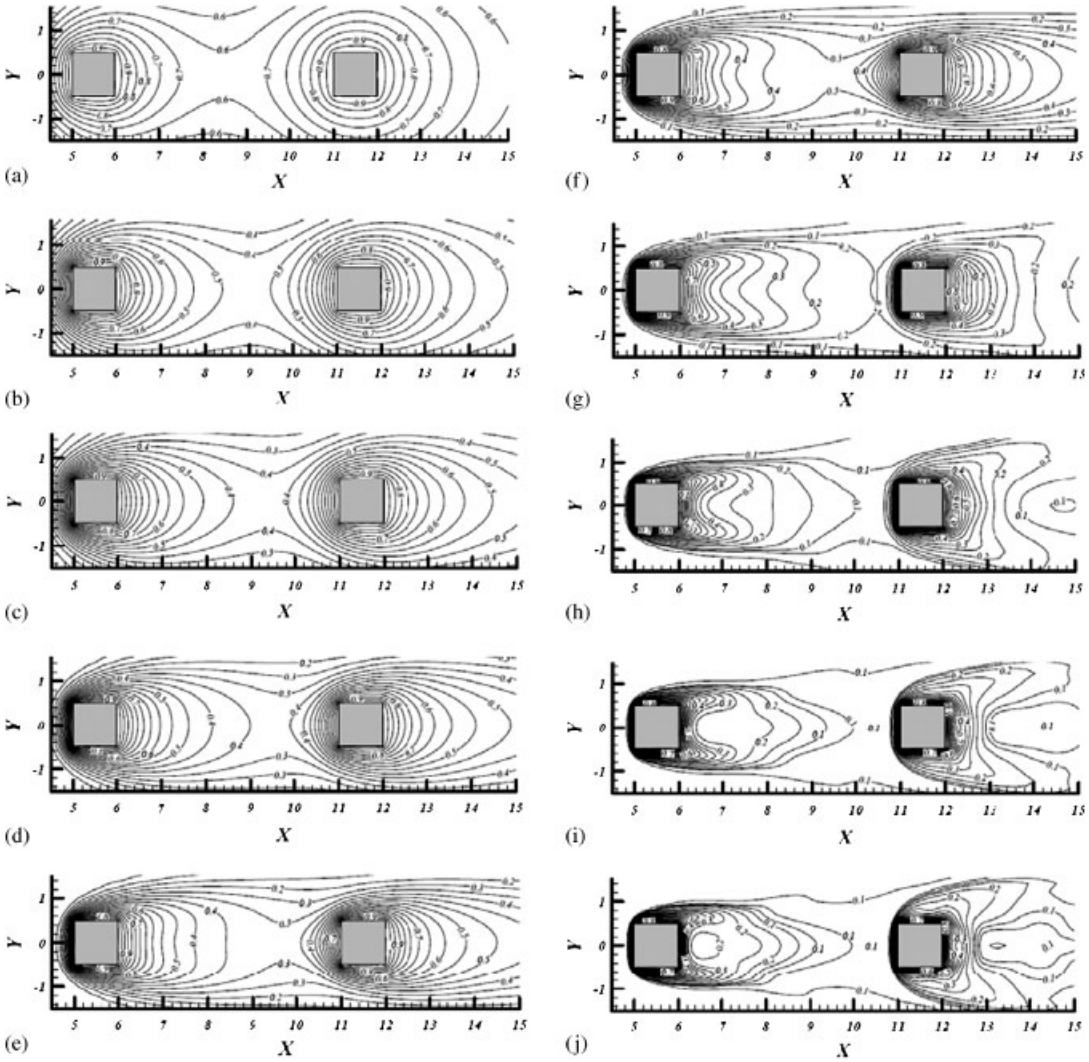

Figure 8. The isotherms around the cylinders for different Reynolds numbers: (a) $Re=1$; (b) $Re=5$; (c) $Re=10$; (d) $Re=20$; (e) $Re=35$; (f) $Re=50$; (g) $Re=70$; (h) $Re=100$; (i) $Re=150$; and (j) $Re=200$. The time-averaged isotherms are shown for the unsteady-periodic flow cases ($Re>35$).

of the drag and lift forces is shown for upstream and downstream cylinders. It is seen that the flow is steady and the forces remain constant during the time, e.g. at $Re=1, \mathrm{Cd}\approx 14.94, \mathrm{Cl}=0$ for upstream cylinder, see Figure 9. In unsteady cases, the forces become periodic and their fluctuations increase with increasing the Reynolds number from the onset one, see Figures 9 and 10.

Figure 10 shows the RMS of forces for both the cylinders. It is seen that the level of the force fluctuations on the downstream cylinder is larger than the corresponding values for the upstream one (see also Figure 9). This is because the flow interaction of the upstream cylinder with the downstream one causes to amplify the forces and their fluctuations. As seen in Figure 10, the RMS

DOI: 10.1002/fld

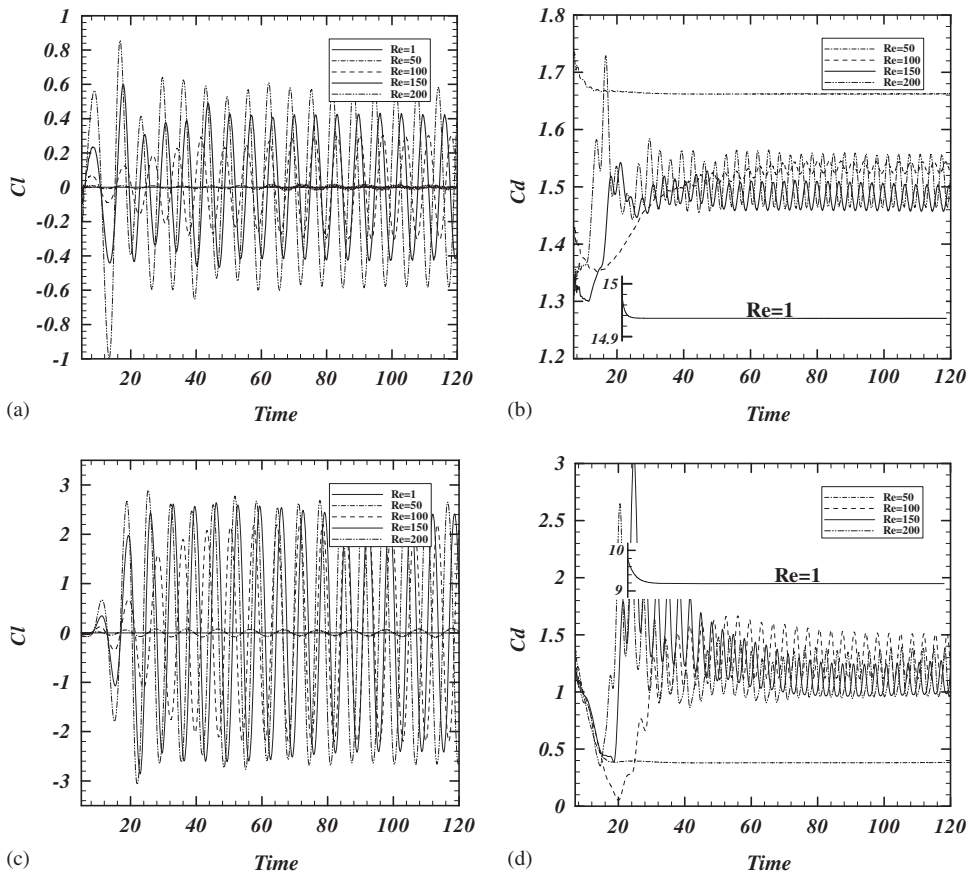

Figure 9. Instantaneous lift and drag coefficients. The upstream cylinder: (a) lift coefficient; (b) drag coefficient, the downstream cylinder; (c) lift coefficient; and (d) drag coefficient.

of lift coefficient for both the cylinders is larger than the corresponding values of the drag one (see also Figure 9). This point is also reported for the flow around a single square cylinder [11–15].

The variations in the recirculation length for both the cylinders are shown in Figure 11. In this figure, the experimental results ($Re = 4.4$–35) for the single circular cylinder [20] and also the numerical results for the single square cylinder [13] are shown. In the steady cases, the recirculation length behind the cylinders becomes larger by increasing the Reynolds number and it reaches to the maximum size at the onset Reynolds number, see Figures 11 and 6(a)–(e). In the unsteady cases, the time-averaged recirculation length at the upstream cylinder decreases by increasing the Reynolds number, while the corresponding value for the downstream cylinder first decreases and then gradually increases, see Figures 11(b) and 6(f)–(j). In all the steady and the unsteady cases, the recirculation length of the upstream cylinder is larger than the corresponding value for the downstream cylinder. The size of the recirculation length of both the cylinders draws very close to a same value at approximately $Re = 200$. Decreasing the recirculation length of the upstream cylinder by increasing the Reynolds number provides more opportunities for the flow to recover pressure before encountering the downstream cylinder.

DOI: 10.1002/fld

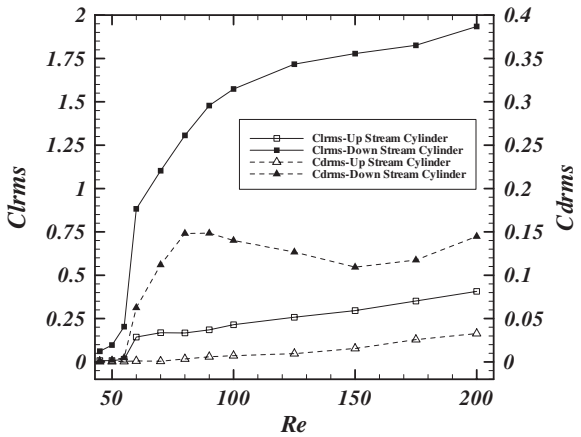

Figure 10. The RMS coefficients versus Reynolds number for upstream and downstream cylinders. The time-averaged values are shown for the unsteady-periodic flow cases ($Re>35$).

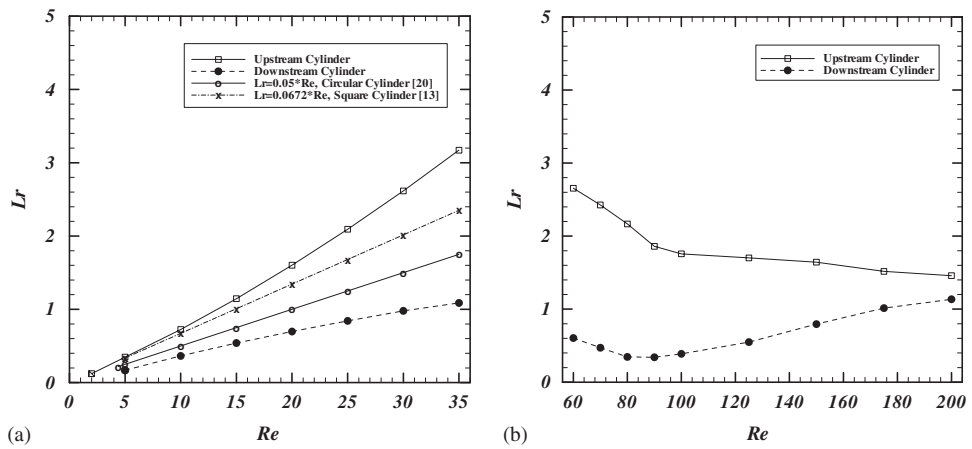

Figure 11. Recirculation length of the cylinders versus Reynolds number: (a) steady and (b) unsteady-periodic flow. The time-averaged values are shown for the unsteady-periodic flow cases ($Re>35$).

From Figure 11, it is also seen that the recirculation length for a single square or circular cylinder increases up to approximately the onset of vortex shedding and then decreases, and the same trend also occurs for the upstream cylinder in the tandem arrangement.

The following expressions for the recirculation length with a maximum deviation of 5% are derived using a linear curve-fit by the least-squares method:

$$\text{Up stream cylinder: } \frac{Lr}{d} = -0.214 + 0.094 \times Re \quad \text{for } 5 \leqslant Re \leqslant 35 \tag{4}$$

$$\text{Down stream cylinder: } \frac{Lr}{d} = 0.056 + 0.031 \times Re \quad \text{for } 5 \leqslant Re \leqslant 35 \tag{5}$$

DOI: 10.1002/fld

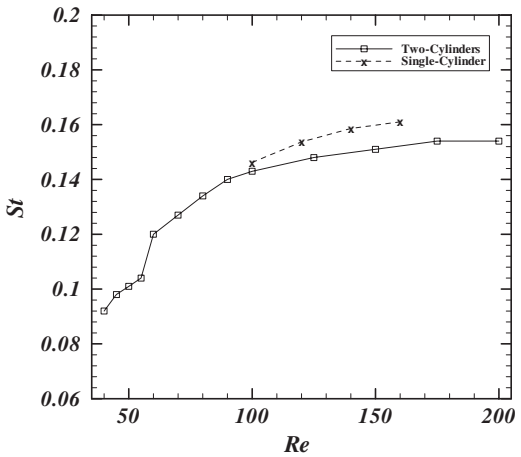

Figure 12. Strouhal number versus Reynolds number.

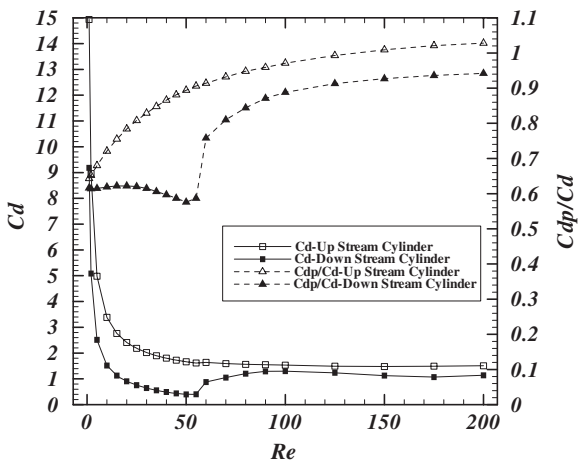

Figure 13. Variation of drag coefficient (left axis) and the ratio of the pressure drag and the total drag coefficients (right axis) for the upstream and downstream cylinders.

Strouhal number (St) is shown for different Reynolds numbers in Figure 12. Strouhal number increases with the increasing of the Reynolds number from the onset one. It is found that the vortex shedding begins at a same onset Reynolds number ($Re = 35$–40) for both the cylinders and St has similar values for both the cylinders at each Reynolds number. There is a sharp variation in St in the range of Reynolds numbers between 55 and 60 due to the change of the flow pattern in the space between the cylinders, see also Figures 6, 7 and 13. This flow pattern also provides similar changes in the other global parameters. Likewise, the changes of the Strouhal number reduces for $Re \geqslant 100$ due to the formation of nearly similar flow pattern around cylinders (Figures 7(h)–(j)).

DOI: 10.1002/fld

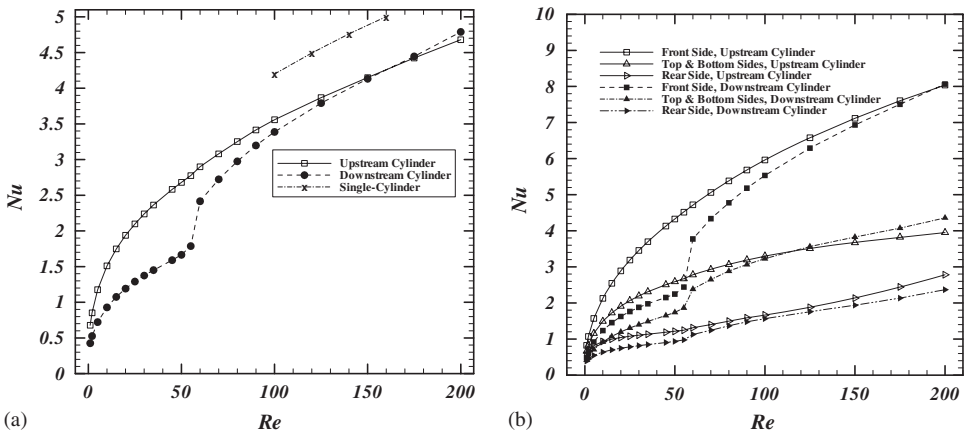

Figure 14. Nusselt number versus Reynolds number for: (a) cylinders and (b) different sides of the cylinders. The time-averaged values are shown for the unsteady-periodic flow cases ($Re>35$).

Strouhal number of the single cylinder is also shown in Figure 12. There is a slight difference between Strouhal number single and tandem ones.

In Figure 13, the drag coefficient versus Reynolds number is shown. At very low Reynolds number ($Re=1$), there is no flow separation and the drag is predominantly a friction drag, see Figure 6. As the Reynolds number is increased from $Re=1$, the flow separation occurs and the drag is a combination of friction and pressure drag. In this case, the pressure drag starts to increase slowly, whereas the friction drag decreases sharply. Thus, the drag coefficient of both the cylinders drops continuously by increasing the Reynolds number up to about $Re=55-60$. The contribution of the pressure drag coefficient is about 80% of the total drag coefficient at $Re=50$. At higher Reynolds number, the drag coefficient of the upstream cylinder is relatively constant, whereas the drag coefficient of the downstream cylinder increases gradually due to the change of flow pattern in the spacing between the cylinders, see Figures 6 and 11. At $Re>100$, the drag coefficient of the downstream cylinders becomes approximately constant and it approaches the corresponding value of the upstream cylinder. It is important to mention that the location of flow separation points changes from the upstream cylinder trailing edges to their leading edges at about $Re>100$. This provides a relatively constant wake and flow pattern, which provides a relatively constant drag force.

The time-averaged Nusselt numbers for the cylinders and also their different sides versus Reynolds number are shown in Figure 14. The results show an increase in the Nusselt number with the Reynolds number. As seen from Figure 14(a), the Nusselt number for the front surface displays the highest value, the top and bottom surface value is intermediate, and the rear surface has the lowest value. The level of Nusselt number for upstream cylinder is higher than the corresponding value for the downstream cylinder. There is a relatively sharp variation in the Nusselt number of the cylinder surfaces of the downstream cylinder in the range of Reynolds numbers between 55 and 60 due to the change of the flow pattern in the space between the cylinders, see also Figures 6, 7 and 13. Change in the flow pattern in the space between the cylinders has the greatest effect on the front side and the least effect on the rear side of the downstream cylinder.

An empirical expression for single circular cylinder Nusselt number is reported with a maximum deviation of 4% with the experimental values in the Reynolds number range from 1 to 4000 as

DOI: 10.1002/fld

follows [21]:

$$Nu = 0.48\sqrt{Re} + 0.43 \tag{6}$$

In [21], it is shown that the Nusselt number for any 2D laminar boundary layer is proportional to the square root of the Reynolds number, if the thickness of boundary layer becomes small. Likewise, a correlation for a single square cylinder Nusselt number is also reported with a maximum deviation of 3% with the computed results in the Reynolds number range from 5 to 160 as follows [13]:

$$Nu = 0.359\sqrt{Re} + 0.442 \tag{7}$$

Similar relations are obtained based on the results of this study:

$$\text{Up stream cylinder: } Nu = 0.299 \times \sqrt{Re} + 0.543 \quad \text{for } 5 \leqslant Re \leqslant 200 \tag{8}$$

$$\text{Down stream cylinder: } \begin{cases} Nu = 0.204 \times \sqrt{Re} + 0.257 & \text{for } 2 \leqslant Re \leqslant 55 \\ Nu = 0.359 \times \sqrt{Re} - 0.267 & \text{for } 60 \leqslant Re \leqslant 200 \end{cases} \tag{9}$$

These correlations are suggested with a maximum deviation of 4% from the results of the present study.

4. CONCLUSION

Fluid flow and heat transfer from the tandem square cylinders in the laminar flow regime are investigated ($1 \leqslant Re \leqslant 200, Pr = 0.71, G = 5$). The results show that the flow is steady for $Re \leqslant 35$ and unsteady-periodic for $Re \geqslant 40$. The onset of vortex shedding occurs in the range of $Re = 35$–40. It is observed that the flow separates from the cylinder rear corners in the range of $1 < Re \leqslant 2$ for the upstream cylinder and $2 < Re \leqslant 5$ for the downstream cylinder. It is found that the location of the flow separation changes from the rear to the frontal corners of the upstream cylinder in the range of $100 < Re \leqslant 125$.

It is found that the level of the force fluctuations on the downstream cylinder is larger than the corresponding values for the upstream one due to the flow interaction of the upstream cylinder with the downstream one.

It is observed that there is a relatively sharp variation in the global parameters of the downstream cylinder in the range of Reynolds numbers between 55 and 60 due to the change of the flow pattern in the space between the cylinders.

It is found that the Nusselt number for the front surface displays the highest value, the top and bottom surface value is intermediate, and the rear surface has the lowest value. The level of Nusselt number for the upstream cylinder is higher than the corresponding value for the downstream cylinder.

A comparison between the results of the single cylinder and the tandem cylinders shows that there are relatively similar results for the single cylinder and the upstream cylinder of the tandem case.

DOI: 10.1002/fld

NOMENCLATURE

B	blockage ratio ($=d/H$), see Figure 1.
Cd	total drag coefficient
Cdp	pressure drag coefficient
$\mathrm{Cd}_{\mathrm{rms}}$	root mean square (RMS) of the drag coefficient
Cl	lift coefficient
$\mathrm{Cl}_{\mathrm{rms}}$	root mean square (RMS) of the lift coefficient
Cp	pressure coefficient
d	width of square cylinders, see Figure 1.
f	frequency of vortex shedding
G	spacing between the cylinders, see Figure 1.
H	width of computational domain, see Figure 1.
h	convective heat transfer coefficient upstream
k	fluid thermal conductivity
L	length of computational domain, see Figure 1.
Lr	recirculation length
M	number of grid points in X direction
N	number of grid points in Y direction
Nu	average Nusselt number ($=hd/k$)
Pr	Prandtl number
Re	Reynolds number ($=u_{\mathrm{in}}d/\upsilon$)
St	Strouhal number ($=fd/u_{\mathrm{in}}$)
t	Time
T	Temperature
T_{in}	free-stream temperature
T_{w}	cylinder walls temperature
u	streamwise velocity
u_{in}	free-stream velocity
U	non-dimensional streamwise velocity ($=u/u_{\mathrm{in}}$)
v	cross-stream velocity
V	non-dimensional cross-stream velocity ($=v/u_{\mathrm{in}}$)
x	streamwise dimension coordinate
X	non-dimensional streamwise dimension coordinate ($=x/d$)
X_d	non-dimensional streamwise distance between the rear side of the downstream cylinder and the exit plane (see Figure 1)
X_u	non-dimensional streamwise distance between the inlet plane and the front side of the upstream cylinder (see Figure 1)
y	cross-stream dimension of coordinate
Y	non-dimensional cross-stream dimension of coordinates ($=y/d$)

Greek letters

α	thermal diffusion coefficient
θ	non-dimensional temperature $[=(T-T_{\mathrm{in}})/(T_{\mathrm{wall}}-T_{\mathrm{in}})]$
ρ	fluid density
v	fluid kinematic viscosity t time

DOI: 10.1002/fld

τ non-dimensional time $[=t/(d/u_{\text{in}})]$
ω vorticity

REFERENCES

1. Lyn DA, Einav S, Rodi W, Park JH. A laser-Doppler velocimetry study of ensemble-averaged characteristics of the turbulent near wake of a square cylinder. *Journal of Fluid Mechanics* 1995; **304**:285–319.
2. Williamson CHK. Three-dimensional wake transition. *Journal of Fluid Mechanics* 1996; **328**:345–407.
3. Sohankar A. Flow over a bluff body from moderate to high Reynolds numbers using large eddy simulation. *Computers and Fluids* 2006; **35**:1154–1168.
4. Tatsutani K, Devarakonda R, Humphrey JAC. Unsteady flow and heat transfer for cylinder pairs in a channel. *International Journal of Heat and Mass Transfer* 1993; **13**:3311–3328.
5. Valencia A. Unsteady flow and heat transfer in a channel with a built-in tandem of rectangular cylinders. *Numerical Heat Transfer*, *Part A* 1996; **26**:613–623.
6. Valencia A. Numerical study of self-sustained oscillatory flows and heat transfer in channels with a tandem of transverse vortex generators. *Heat and Mass Transfer* 1998; **33**:465–470.
7. Rosales JL, Ortega A, Humphrey JAC. A numerical simulation of the convective heat transfer in confined channel flow past square cylinders: comparison of inline and offset tandem pairs. *International Journal of Heat and Mass Transfer* 2001; **44**:587–603.
8. Liu CH, Chen JM. Observations of hysteresis in flow around two square cylinders in a tandem arrangement. *Journal of Wind Energy and Industrial Aerodynamics* 2002; **90**:1019–1050.
9. Alam MDM, Moriya M, Takai K, Sakamoto H. Suppression of fluid forces acting on two square prisms in a tandem arrangement by passive control flow. *Journal of Fluids and Structures* 2002; **16**:1073–1086.
10. Yen SC, San KC, Chuang TH. Interactions of tandem square cylinders at low Reynolds numbers. *Experimental Thermal and Fluid Science* 2008; **32**:927–938.
11. Sohankar A, Norberg C, Davidson L. Low-Reynolds-number flow around a square cylinder at incidence: study of blockage, onset of vortex shedding and outlet boundary condition. *International Journal for Numerical Methods in Fluids* 1998; **26**:39–56.
12. Thompson JF, Warsi ZUA, Mastin CW. *Numerical Grid Generation*, *Foundations and Applications*. Elsevier: New York, 1985; 305–310.
13. Sharma A, Eswaran V. Heat and fluid flow across a square cylinder in the two-dimensional laminar flow regime. *Numerical Heat Transfer*, *Part A* 2004; **45**:247–269.
14. Sohankar A, Norberg C, Davidson L. Numerical simulation of unsteady low-Reynolds number flow around rectangular cylinders at incidence. *Journal of Wind Energy and Industrial Aerodynamics* 1997; **69**:189–201.
15. Sohankar A, Davidson L, Norberg L. Numerical simulation of unsteady flow around a square 2D cylinder. In *Proceedings of the 12th Australasian Fluid Mechanics Conference*, Bilger RW (ed.). 1995; 517–520.
16. Robichaux J, Balachandar S, Vanka SP. Two-dimensional Floquet instability of the wake of square cylinder. *Physics of Fluids* 1999; **11**:560–578.
17. Franke R, Rodi W, Schönung B. Numerical calculation of vortex shedding flow past cylinders. *Journal of Wind Energy and Industrial Aerodynamics* 1990; **35**:237–257.
18. Shimizu Y, Tanida Y. Fluid forces acting on cylinders of rectangular cross section. *Transactions of the Japan Society of Mechanical Engineering B* 1978; **44**:2699–2706.
19. Kelkar KM, Patankar EF. Numerical prediction of vortex shedding behind a square cylinder. *International Journal for Numerical Methods in Fluids* 1992; **14**:327.
20. Zdravkovich MM. *Flow Around Circular Cylinders*. Oxford University Press: New York, 1997.
21. Eckert ERG, Soehngen E. Distribution of heat transfer coefficient around circular cylinders in cross flow at Reynolds numbers from 20 to 500. *Journal of Heat Transfer* 1952; **74**:343–347.

DOI: 10.1002/fld